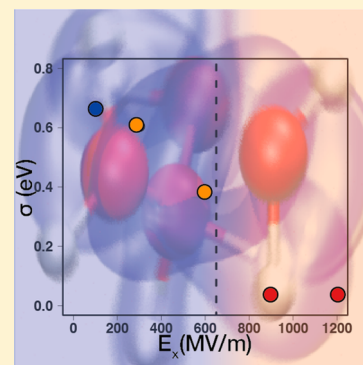


Field-Induced Carrier Localization Transition in Dielectric Polymers

Thomas M. Linker,[†] Subodh Tiwari,[†] Hiroyuki Kumazoe,[‡] Shogo Fukushima,[‡] Rajiv K. Kalia,[†] Aiichiro Nakano,^{*,†} Rampi Ramprasad,[§] Fuyuki Shimojo,[‡] and Priya Vashishta[†][†]Collaboratory for Advanced Computing and Simulations, University of Southern California, Los Angeles, California 90089-0242, United States[‡]Department of Physics, Kumamoto University, Kumamoto 860-8555, Japan[§]School of Materials Science and Engineering, Georgia Institute of Technology, Atlanta, Georgia 30332, United States

Supporting Information

ABSTRACT: Organic polymers offer many advantages as dielectric materials over their inorganic counterparts because of high flexibility and cost-effective processing, but their application is severely limited by breakdown in the presence of high electric fields. Dielectric breakdown is commonly understood as the result of avalanche processes such as carrier multiplication and defect generation that are triggered by field-accelerated hot carriers (electrons or holes). In stark contrast to inorganic dielectric materials, however, there remains no mechanistic understanding to enable quantitative prediction of the breakdown field in polymers. Here, we perform systematic study of different electric fields on hot carrier dynamics and resulting chemical damage in a slab of archetypal polymer, polyethylene, using nonadiabatic quantum molecular dynamics simulations. We found that high electric fields induce localized electronic states at the slab surface, with a critical transition occurring near the experimentally reported intrinsic breakdown field. This transition in turn facilitates strong polaronic coupling between charge carriers and atoms, which is manifested by severe damping of the time evolution of localized states and the presence of C–H vibrational resonance in the hot-carrier motion leading to rapid carbon–carbon bond breaking on the surface. Such polaronic localization transition may provide a critically missing prediction method for computationally screening dielectric polymers with high breakdown fields.



The use of polymers as dielectric materials in electronic circuits offer many advantages over typically used inorganic materials as they are highly flexible and are able to be cheaply produced,^{1–3} but their application is severely limited by their electronic breakdown in the presence of high electric fields.^{4,5} For inorganic materials, dielectric breakdown under electric field is well-described by electron avalanche theory.^{6–8} Formulated by the early works of Zener,⁹ Frölich,¹⁰ and Von Hippel,¹¹ avalanche theory describes the onset of electrical breakdown when the applied field accelerates electrons past the impact ionization energy, which in turn causes further excitation of hot carriers (electrons or holes). This avalanche process then results in structural damage of the material such as crack formation.^{4,5} In this model, the critical field for breakdown can be determined by solving the energy balance equation between the energy gain by the applied field and the energy loss due to electron–phonon scattering.^{6–8} Breakdown in organic materials like polymers is expected to follow an avalanche process similar to inorganic materials, but no such theory exists to predict the critical field. The difficulty partly arises from the strong coupling between charge carriers and atomic motions (or phonons) in polymers. In the case of inorganic solids, weak carrier–phonon coupling allows the use of perturbation theory to estimate the critical field.^{7,8,12,13} In polymers, in contrast, strong carrier–phonon interaction leads

to polaronic effects,¹⁴ thus precluding the use of the well-established perturbation theory for critical-field estimation. Consequently, state-of-the-art computational screening for rational design of high-performance dielectric polymers heavily relies on a qualitative proxy (i.e., electronic band gap) of the breakdown field.²

For quantitative estimation of the breakdown field in polymers, which is critically missing, it is essential to mechanistically understand field-induced hot carrier dynamics. First-principles simulations based on nonadiabatic quantum molecular dynamics (NAQMD) started shedding some light on this topic (see [Methods](#)). Recently, Kumazoe et al.¹⁵ performed NAQMD simulations to identify key field-induced hot-carrier processes in a polyethylene (PE) slab, which is one of the most extensively studied and widely produced polymers.^{4,15–18} Under an electric field of 600 MV/m, they observed carrier multiplication and bond deformation as a result of hot carrier excitation. However, an exhaustive study of the effect of both pre- and post-breakdown fields on hot carrier processes in PE has yet to be performed. The key scientific question is: What determines the breakdown field in polymers?

Received: October 25, 2019

Accepted: December 21, 2019

Published: December 21, 2019

We found a field-induced carrier-localization transition at a critical field of ~ 600 MV/m, which in turn strengthens carrier–phonon coupling, thereby leading to chemical damage. This Letter elucidates the electronic origin of the polaronic localization transition.

While the earlier NAQMD work¹⁵ has laid a microscopic foundation to study rich carrier dynamics under strong electric fields, it lacked a predictive power such as quantitative assessment of the breakdown field. The present work not only finds a new phenomenon of field-induced carrier localization transition in polymers but also proposes the use of thus-found critical field strength as a quantitative measure for screening dielectric polymers with high breakdown fields. While the Stark shift of electronic energy levels under an electric field has been known for a century,¹⁹ its resonance with vibrational excitations and their spatial localization were recognized relatively recently.²⁰ The present work for the first time points out that similar resonance gives rise to a sharp localization transition at a critical field strength in polymers.

To systematically study the effects of electric fields on carrier dynamics in PE, we performed NAQMD simulations on a PE slab consisting of $18 \times 1 \times 2$ unit cells composed of 36 PE chains. Figure 1a shows (001) (or xy) plane view of the PE slab, whereas Figure S1 in the Supporting Information shows

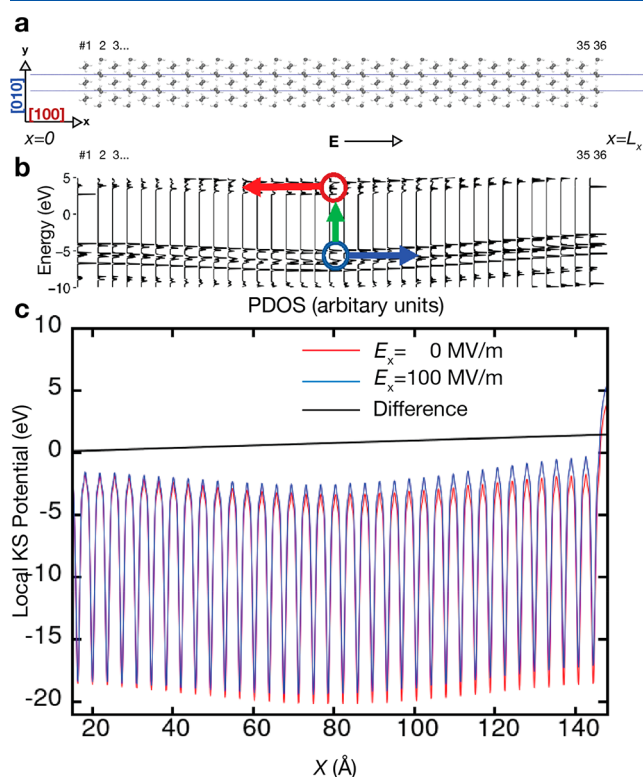


Figure 1. Polyethylene (PE) under electric field. (a) (001) (or xy)-plane view of the PE slab, where PE chains are numbered from 1 to 36 with respect to their positions along the [100] direction. (b) Partial density of states (PDOS) projected onto the 36 PE chains under an electric field of 100 MV/m. Schematic of excitation is shown, where blue and red circles represent hole and electron, respectively. Blue and red arrows show the respective direction of travel of hole and electron. (c) Response of the local Kohn–Sham (KS) potential to the applied electric field. Blue and red curves show the KS potential profile along the [100] direction with and without electric field, respectively, whereas the black curve shows their difference.

its (010) (or xz) view. PE chains are orientated along the [001] direction and are numbered from 1 to 36 with respect to their position along the [100] direction. An additional 15 Å of vacuum was applied along the [100] direction on both sides (total 30 Å) as shown in Figure 1a. Electric fields were applied in the [100] direction (left to right in Figure 1a) using a sawtooth potential. Figure 1b shows the spatially projected partial density states (PDOS) on each polymer chain along the [100] direction for PE under a 100 MV/m electric field. In the PDOS we observe a superposition of bending due to the exposed surface^{21,22} and tilting due to the linear voltage drop arising from applied electric field as shown in Figure 1b. Figure S2 shows the PDOS of the PE slab in the presence of 0, 100, 300, 600, 900, and 1200 MV/m electric fields. The resulting PDOS is tilted near the surface on the right edge of the supercell because of the applied positive electric field, while the left edge displays a flat band profile due to the mixture of band tilting and linear voltage drop. These effects are more pronounced in the higher electric fields (Figure S2).

The linear voltage drop can be seen more clearly by examining the change of the local Kohn–Sham (KS) potential profile due to the applied electric field. Figure 1c compares the (100) plane-averaged local KS potential with an applied electric field of 100 MV/m (blue curve) with that without electric field (red curve). Their difference (black curve) represents change in potential due to the applied electric field. The local KS potential responds linearly to the applied electric field.

To simulate carrier excitation, an electron is excited from the valence band in the bulk of the material to the conduction band, thereby creating an electron–hole pair. The hole behaves as a positively charged particle and thus moves toward $x = L_x$, indicated with the blue arrow in Figure 1b, where L_x is the length of the supercell along the [100] direction. In contrast, the excited electron moves toward $x = 0$ as schematically shown by the red arrow in Figure 1b. Because the band profile near $x = 0$ is relatively flat as mentioned before, the electron experiences relatively less driving force by the electric field, and thus, the hole dictates the breakdown processes.

To investigate the effect of different electric fields, panels a, b, and c of Figure 2 shows time evolution of the KS eigenvalues for fields of 100, 600, and 900 MV/m, respectively. After excitation at time $t = 0$, an electron–hole pair is generated. As a result, an unstable high-energy state is formed, causing the hole energy (blue curve) to relax to the valence band maximum (VBM) while the excited electron energy (red curve) to relax to the conduction band minimum (CBM) rapidly within 50–100 fs, as shown in Figure 2a–c. The rapid carrier relaxation itself is a general phenomenon even in the absence of electric field, as shown in Figure S3. Under a 100 MV/m field the hole undergoes rapid and decoherent motion and does not localize to any particular electronic band or spatial location. The rapid oscillation in the hole dynamics, shown in Figure 2a, was found to result from high-frequency transitions between highly degenerate KS eigenstates (see Figure S4 in the Supporting Information). For $E = 600$ MV/m, this high-frequency motion is still present, but after relaxation the hole localizes to the VBM from $t = 125$ –155 fs and after $t = 190$ fs. During these periods the VBM wave function forms a gap state as it separates from the rest of the KS states. Under the application of a 900 MV/m field, a transition occurs from decoherent hole motion to coherent motion occurs, as the hole

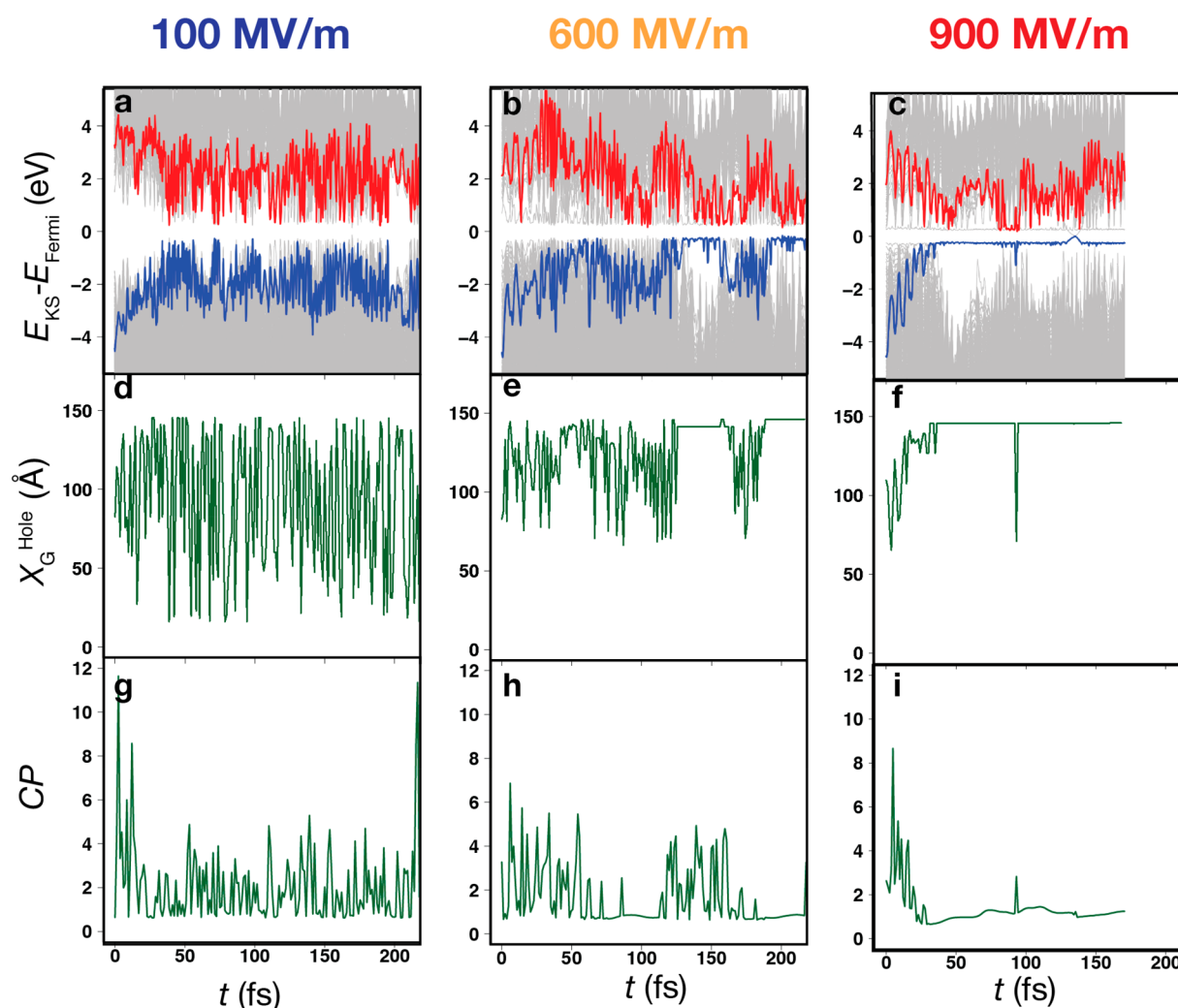


Figure 2. Hole relaxation and localization. (a–c) Time evolution of KS eigenvalues under electric fields of 100 MV/m (a), 600 MV/m (b) and 900 MV/m (c). The blue and red curves are the hole and electron eigenenergies, respectively. (d–f) Center-of-mass (COM) position of the hole, X_G^{Hole} , along the [100] direction for 100 MV/m (d), 600 MV/m (e) and 900 MV/m (f). (g–i) Chain participation number, CP, of the hole for 100 MV/m (g), 600 MV/m (h) and 900 MV/m (i).

smoothly relaxes to the VBM with a clear dominant frequency. This is then followed by the immediate formation and sustainment of a gap state at $t = 40$ fs. Fourier transformation of the hole eigenenergy between 0 and 40 fs shows a peak near 200 THz, which is close to twice the C–H stretching frequency (92 THz), as shown in Figures S5 and S6. The second C–H harmonic reflects the deviation of the C–H bond length from its equilibrium values, which oscillates at twice the C–H stretching frequency, as was found in a previous study of quaterthiophene on a zinc-oxide surface.²³ The same harmonic is present in the hole time evolution under a field of 1200 MV/m (Figure S6). Similar C–H harmonic resonance may also be present in lower electric fields but is washed out by the high frequency of electronic transitions due to KS state degeneracy, which is discussed in the Supporting Information.

To understand the formation of these gap states, we further investigated the center-of-mass (COM) position of the hole along the [100] direction as a function of time. For the k th KS wave function $\Psi_k(\mathbf{r}, t)$, the COM position can be calculated as

$$X_G^k = \frac{L_x}{2\pi} \text{Im} \left[\text{Log} \left(\int_{\Omega} d^3r |\Psi_k(\mathbf{r}, t)|^2 \exp \left(\frac{2\pi i}{L_x} x \right) \right) \right] \quad (1)$$

where L_x is the length of the supercell along the [100] direction and Ω is the volume of the supercell. We also calculated the chain participation number (CP) of hole for each applied electric field: $CP = \sum_i 1/p_i^2$, where p_i is the probability the hole is on the i^{th} PE chain. Figure 2d–f shows the time evolution of the hole COM position, whereas Figure 2g–i shows that of the CP value. The 100 MV/m field does not induce any gap states, suggesting a highly delocalized hole in the system, as shown in Figure 2d,h. The gap states formed under 600 and 900 MV/m fields correspond to spatial localization of the hole at the surface and its confinement to a single PE chain, indicated by the CP value near unity. In addition, the hole's physical motion to the surface appears to undergo a similar coherent motion found in its eigenenergy evolution. We found a peak frequency near 200 THz in the carrier motion, which is consistent with earlier discussed C–H vibrational resonance in the hot carrier motion. This coherent frequency was also seen in PE under a 1200 MV/m field (Figure S8). The presence of this frequency in both the energy and spatial evolution of the hole indicates that C–H vibrational modes assist the carrier motion to the surface under these high electric fields.

This transition from decoherent to coherent motion under increased electric fields indicates a critical transition occurring past 600 MV/m, which is near the reported breakdown field for PE. Experimental short-term breakdown of polymers is expected to follow a statistical distribution,²⁴ where the average experimental value for intrinsic breakdown is reported in the range of 550–650 MV/m.^{5,25} With increased electric field, we observed decoupling of the VBM eigenstate from the remaining KS states prior to hot-carrier relaxation, which displays an energy profile similar to the gap states formed when the hole localized on the surface of the slab (Figure S6). This indicates that high electric field induces localized states at the surface of the PE slab before the hot-carrier relaxation.

To quantify this localization transition, we examined the spatial position of the VBM wave function along the [100] direction for the first 50 fs of the simulation as shown in Figure 3a–c. As the field increases, the VBM wave function becomes

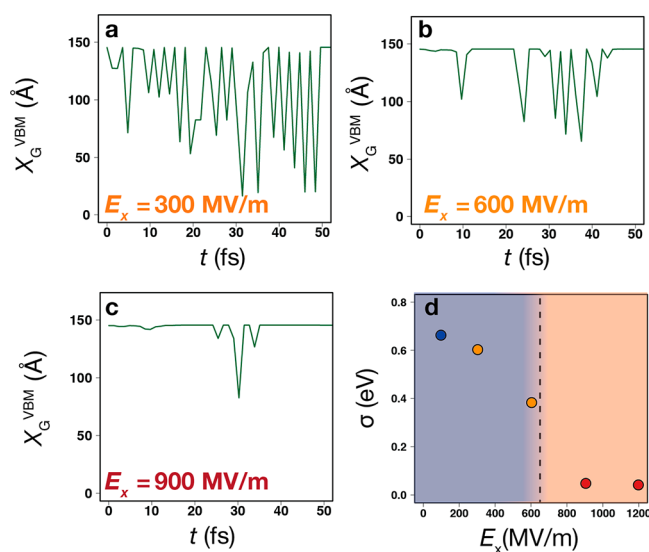


Figure 3. Field-induced localization. Panels a–c show the expectation value of the position VBM wave function along the [100] or x direction during the first 50 fs for fields of 300, 600, and 900 MV/m, respectively. Panel d shows the energy fluctuation of the VBM wave function versus the electric field.

increasingly localized to the surface of the slab. By inducing a localized state at the surface of the slab, high electric fields increase the susceptibility for the hole to localize on the surface upon relaxation. For PE under an electric field of 1200 MV/m, the localization of the VBM wave function was delayed. This resulted in a delay of the emergence of the coherent carrier motion and in formation of a sustained gap state (Figure S7). A critical transition occurs past 600 MV/m, where the VBM wave function becomes extremely localized to the surface and decoupled from the other states, followed by coherent motion of the hole to the surface. This transition is well quantified by the fluctuation (σ) of the VBM energy before hole localization as a function of applied field (Figure 3d). Figure 3d exhibits a phase-change-like transition, where 900 and 1200 MV/m fields extremely dampen the VBM energy in comparison to the lower fields. This extreme dampening corresponds to a highly localized state at the surface decoupled from the remaining KS states. The degeneracy of KS states is broken by the extreme electric fields, resulting in coherent motion of the hole to surface followed by sustained localization.

The extreme localization of the hole on the surface and formation of the gap state results in the chemical damage to the PE slab. Figure 4 shows the C–C bond lengths for PE

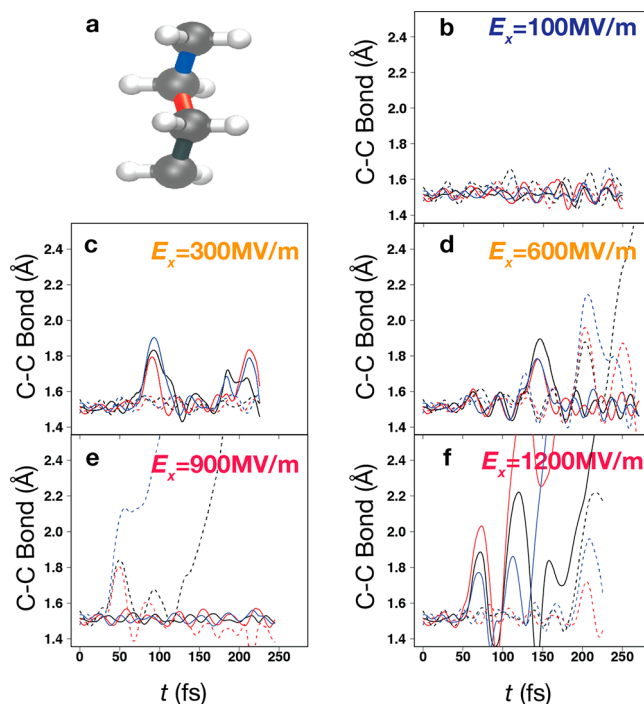


Figure 4. Bond stretching and breaking. (a) Three distinct bonds colored black, red, and blue present in PE chains. Dark gray and white spheres represent carbon (C) and hydrogen (H), respectively. (b–f) Time evolution of C–C bond lengths for surface chains 35 (solid curve) and 36 (dashed curve). Black, red, and blue curves represent same colored bond in panel a.

chains 35 (solid curves) and 36 (dashed curves) as a function of time under all five applied electric fields. For a field of 100 MV/m, no localized gap state is formed and accordingly no bond stretching or breaking occurs at the surface. For 300 MV/m, two gap states were formed briefly at $t = 90$ –115 fs and $t = 195$ –210 fs (Figure S9) resulting in a localization of the hole on polymer chain 35. These gap states resulted in weakening of C–C bonds and hence increased C–C bond length on the 35th chain. The 600 MV/m field induced the formation of localized gap states at $t = 125$ fs on polymer chain 35 leading to more extreme bond-stretching. Further, at $t = 200$ fs, the hole localized on chain 36 for a longer time (50 fs) leading to a C–C bond cleavage. Past the critical transition shown in Figure 3d, we observed formation of a highly localized gap state immediately after the hole reaches the surface, resulting in rapid destruction of C–C bonds at the surface for PE under 900 and 1200 MV/m fields, as shown in panels e and of Figure 4, respectively. The electric field has a 2-fold effect on the chemical damage in PE by first inducing a localized occupied state at the surface that increases the susceptibility of the hole to localize at the surface after relaxation. After hole localization to the surface, surface C–C bonds become depopulated making them more susceptible to being broken by the electric field. Once broken, the resulting defects will change the charge dynamics inside the polymer triggering a positive feed-back breakdown process.²⁶ While weaker fields here caused limited chemical damage, long-term exposure to them could eventually result in breakdown due to

the process known as polymer aging. Experimental evidence suggests chemical aging may occur as a result of energy release due to electron–hole recombination on time scales out of reach for NAQMD simulations.^{27,28}

In summary, we have performed an exhaustive investigation of the effects of electric fields in PE. We observed that high electric fields lift the degeneracy of the PE slab by inducing a highly localized state at the slab surface. This increases the susceptibility for the hot carrier to localize during carrier relaxation. Upon localization, a high-energy gap state will form, resulting in bond stretching and breaking. We found a critical transition in the response of PE to the applied electric field occurring after 600 MV/m, which is near the known intrinsic breakdown field for PE. This transition is marked by an extreme damping of the VBM energy fluctuation and the presence of C–H vibrational resonance in the hot carrier motion. The polaronic localization transition found here may provide a critically missing prediction method for computationally screening dielectric polymers with high breakdown fields.

While the field-induced polaronic localization transition plays an important role in quantitatively understanding DC electric breakdown, electrical breakdown in dynamic settings (e.g., AC, impulse, and ramp voltage) brings in far richer phenomena. Recent studies have shown the importance of space-charge dynamics in the discrepancies between AC and DC breakdown fields, with AC breakdown field being significantly lower.^{29,30} In addition, the dynamics of space charge and its buildup have been linked to the increase in breakdown strength with rising ramp voltage.²⁵ In the light of Stark effects on the resonance and localization of electronic and vibrational excitations mentioned earlier, such time variation of electric field brings in additional parameters (e.g., AC frequency, ramp rate, and pulse shape) to selectively control specific vibrational modes.³¹

In addition to the time variation of the external field, various factors essentially influence the complex phenomena of experimentally observed dielectric breakdown. These include temperature⁵ and materials properties such as degree of crystallinity, molecular mass, and sample thickness. For example, experimental work by Mason et al. showed an inverse relationship between sample thickness and dielectric breakdown field,³² which was theoretically ascribed to the formation of space charge and its dynamics.²⁵ NAQMD simulations could provide microscopic constitutive parameters into such macroscopic transport models.

Furthermore, chemical defects commonly present in polymer samples likely influence dielectric breakdown. First, they are expected to alter the dielectric properties of polymers. Recent first-principles calculations have shown that defects such as iodine increase the high-frequency dielectric constant of PE, while those involving hydroxyl and carboxyl groups cause anisotropic changes in the static dielectric constant.³³ Chemical impurities are also expected to introduce localized states in the band gap, which can have adverse effects on properties such as polymer aging.^{27,28} The effects of specific defects on hot carrier dynamics and chemical damage in PE will be the subject of future investigation.

METHODS

In this work, we performed NAQMD simulations to understand the process of dielectric breakdown in PE. Quantum molecular dynamics^{34,35} (QMD) is an ab initio

method that integrates the trajectories of all atoms by computing their intermolecular forces from first-principles in the framework of density functional theory^{36,37} (DFT). To approximate the exchange–correlation functional in our DFT approach we used the generalized gradient approximation³⁸ (GGA) and also employed the DFT-D method³⁹ to make corrections for van der Waals interactions. The projected argument wavevector⁴⁰ (PAW) method was used to calculate electronic states. PAW is an all-electron method for computing electronic structure within the frozen core approximation. Projector functions were generated for the carbon 2s and 2p states and the 1s state for hydrogen. Nonadiabatic quantum molecular dynamics^{41–45} (NAQMD) allowed for dynamics of excited carriers to be modeled within the framework of time-dependent DFT⁴⁶ (TDDFT). Excited-state transitions were modeled using the fewest switches surface hopping approach.^{47,48}

Our simulations were employed on a polymer slab consisting of $18 \times 1 \times 2$ unit cells of PE. The equations of motion were integrated in the presence of a Nosé–Hoover thermostat in the canonical ensemble at 300 K. A time step of 0.2418 fs was used, and the Γ point was used to sample the Brillouin zone. The electric field was applied using a sawtooth potential. In this work, we studied the effects of different electric fields on PE ranging from a relatively weak field of 100 MV/m to extreme fields of 900 and 1200 MV/m. The extreme fields were chosen because we are investigating perfect crystalline PE, which will have a higher breakdown field than observed in experiment. The extreme fields ensured we completely captured all the processes involved in dielectric breakdown and allowed us to distinguish the dynamics of hot carriers in pre- and post-breakdown fields. The NAQMD algorithm was implemented in QXMD quantum molecular dynamics simulation code.⁴⁹

ASSOCIATED CONTENT

Supporting Information

The Supporting Information is available free of charge at <https://pubs.acs.org/doi/10.1021/acs.jpcllett.9b03147>.

Additional discussion of electronic relaxation in the absence of electric field, high-frequency hole motion under low electric field, transition to coherent motions, and field-induced localization in 1200 MV/m field (PDF)

AUTHOR INFORMATION

Corresponding Author

*E-mail: anakano@usc.edu.

ORCID

Subodh Tiwari: 0000-0002-5516-6900

Aiichiro Nakano: 0000-0003-3228-3896

Rampi Ramprasad: 0000-0003-4630-1565

Priya Vashishta: 0000-0003-4683-429X

Author Contributions

T.M.L. and S.T. contributed equally to this work. R.K.K., A.N., F.S., R.R., and P.V. designed the research. T.M.L. and S.T. performed the NAQMD simulations. All participated in the analysis of the data and writing the manuscript

Notes

The authors declare no competing financial interest.

ACKNOWLEDGMENTS

This work was supported by the Office of Naval Research through a Multi-University Research Initiative (MURI) grant (N00014-17-1-2656). The simulations were performed at the Argonne Leadership Computing Facility under the DOE INCITE and Aurora Early Science programs and at the Center for High Performance Computing of the University of Southern California

REFERENCES

- (1) Baojin Chu, X. Z.; Ren, K.; Neese, B.; Lin, M.; Wang, Q.; Bauer, F.; Zhang, Q. M. A Dielectric Polymer with High Electric Energy Density and Fast Discharge Speed. *Science* **2006**, *313*, 334–336.
- (2) Sharma, V.; et al. Rational Design of All Organic Polymer Dielectrics. *Nat. Commun.* **2014**, *5*, 4845.
- (3) Su, H.; Strachan, A.; Goddard, W. A. Density Functional Theory and Molecular Dynamics Studies of the Energetics and Kinetics of Electroactive Polymers: PvdF and P(VdF-Trfe). *Phys. Rev. B: Condens. Matter Mater. Phys.* **2004**, *70*, No. 064101.
- (4) Jones, J. P.; Llewellyn, J. P.; Lewis, T. J. The Contribution of Field-Induced Morphological Change to the Electrical Aging and Breakdown of Polyethylene. *IEEE Trans. Dielectr. Electr. Insul.* **2005**, *12*, 951–966.
- (5) Ieda, M. Dielectric Breakdown Process of Polymers. *IEEE Trans. Electr. Insul.* **1980**, *15*, 206–224.
- (6) Sun, Y.; Bealing, C.; Boggs, S.; Ramprasad, R. 50+ Years of Intrinsic Breakdown. *IEEE Electrical Insulation Magazine* **2013**, *29*, 8–15.
- (7) Sparks, M.; Mills, D. L.; Warren, R.; Holstein, T.; Maradudin, A. A.; Sham, L. J.; Loh, E.; King, D. F. Theory of Electron-Avalanche Breakdown in Solids. *Phys. Rev. B: Condens. Matter Mater. Phys.* **1981**, *24*, 3519–3536.
- (8) Sun, Y.; Boggs, S. A.; Ramprasad, R. The Intrinsic Electrical Breakdown Strength of Insulators from First Principles. *Appl. Phys. Lett.* **2012**, *101*, 132906.
- (9) Zener, C. A Theory of the Electrical Breakdown of Solid Dielectrics. *Proc. R. Soc. London, Ser. A* **1934**, *145*, 523–529.
- (10) Frohlich, A. Theory of Electrical Breakdown in Ionic Crystals. *Proceedings of the Royal Society A* **1937**, *160*, 230–241.
- (11) Von Hippel, A. Electric Breakdown of Solid and Liquid Insulators. *J. Appl. Phys.* **1937**, *8*, 815–832.
- (12) Kim, C.; Paliana, G.; Ramprasad, R. From Organized High-Throughput Data to Phenomenological Theory Using Machine Learning: The Example of Dielectric Breakdown. *Chem. Mater.* **2016**, *28*, 1304–1311.
- (13) Kim, C.; Ramprasad, R. Dielectric Breakdown Field of Strained Silicon under Hydrostatic Pressure. *Appl. Phys. Lett.* **2017**, *111*, 112904.
- (14) Cubero, D.; Quirke, N. Computer Simulations of Localized Small Polarons in Amorphous Polyethylene. *J. Chem. Phys.* **2004**, *120*, 7772–7778.
- (15) Kumazoe, H.; Fukushima, S.; Tiwari, S.; Kim, C.; Huan, T. D.; Kalia, R. K.; Nakano, A.; Ramprasad, R.; Shimojo, F.; Vashishta, P. Hot-Carrier Dynamics and Chemistry in Dielectric Polymers. *J. Phys. Chem. Lett.* **2019**, *10*, 3937–3943.
- (16) Bealing, C. R.; Ramprasad, R. An Atomistic Description of the High-Field Degradation of Dielectric Polyethylene. *J. Chem. Phys.* **2013**, *139*, 174904.
- (17) Chen, L. H.; Tran, H. D.; Ramprasad, R. Atomistic Mechanisms for Chemical Defects Formation in Polyethylene. *J. Chem. Phys.* **2018**, *149*, 234902.
- (18) Chen, L. H.; Tran, H. D.; Wang, C. C.; Ramprasad, R. Unraveling the Luminescence Signatures of Chemical Defects in Polyethylene. *J. Chem. Phys.* **2015**, *143*, 124907.
- (19) Stark, J. Observation of the Separation of Spectral Lines by an Electric Field. *Nature* **1913**, *92*, 401.
- (20) Persson, B. N. J.; Avouris, P. The Effects of the Electric Field in the Stm on Excitation Localization - Implications for Local Bond Breaking. *Chem. Phys. Lett.* **1995**, *242*, 483–489.
- (21) Zhang, Z.; Yates, J. T. Band Bending in Semiconductors: Chemical and Physical Consequences at Surfaces and Interfaces. *Chem. Rev.* **2012**, *112*, 5520–5551.
- (22) Kwon, S. K.; Nabi, Z.; Kádas, K.; Vitos, L.; Kollár, J.; Johansson, B.; Ahuja, R. Surface Energy and Stress Release by Layer Relaxation. *Phys. Rev. B: Condens. Matter Mater. Phys.* **2005**, *72*, 235423.
- (23) Mou, W.; Ohmura, S.; Shimojo, F.; Nakano, A. Molecular Control of Photoexcited Charge Transfer and Recombination at a Quaterthiophene/Zinc Oxide Interface. *Appl. Phys. Lett.* **2012**, *100*, 203306.
- (24) Chauvet, C.; Laurent, C. Weibull Statistics in Short-Term Dielectric Breakdown of Thin Polyethylene Films. *IEEE Trans. Electr. Insul.* **1993**, *28*, 18–29.
- (25) Chen, G.; Zhao, J.; Li, S.; Zhong, L. Origin of Thickness Dependent DC Electrical Breakdown in Dielectrics. *Appl. Phys. Lett.* **2012**, *100*, 222904.
- (26) Sun, L.; Marrocchelli, D.; Yildiz, B. Edge Dislocation Slows Down Oxide Ion Diffusion in Doped CeO₂ by Segregation of Charged Defects. *Nat. Commun.* **2015**, *6*, 6294.
- (27) Wang, C. C.; Paliana, G.; Boggs, S. A.; Kumar, S.; Breneman, C.; Ramprasad, R. Computational Strategies for Polymer Dielectrics Design. *Polymer* **2014**, *55*, 979–988.
- (28) Huan, T. D.; Boggs, S.; Teyssedre, G.; Laurent, C.; Cakmak, M.; Kumar, S.; Ramprasad, R. Advanced Polymeric Dielectrics for High Energy Density Applications. *Prog. Mater. Sci.* **2016**, *83*, 236–269.
- (29) Zhou, C.; Chen, G. Space Charge and AC Electrical Breakdown Strength in Polyethylene. *IEEE Trans. Dielectr. Electr. Insul.* **2017**, *24*, 559–566.
- (30) Li, S.; Zhu, Y.; Min, D.; Chen, G. Space Charge Modulated Electrical Breakdown. *Sci. Rep.* **2016**, *6*, 32588.
- (31) Levis, R. J.; Menkir, G. M.; Rabitz, H. Selective Bond Dissociation and Rearrangement with Optimally Tailored, Strong-Field Laser Pulses. *Science* **2001**, *292*, 709–713.
- (32) Mason, J. Breakdown of Solid Dielectrics in Divergent Fields. *Proc. Inst. Electr. Eng., Part C* **1955**, *102*, 254.
- (33) Fukushima, S.; Tiwari, S.; Kumazoe, H.; Kalia, R. K.; Nakano, A.; Shimojo, F.; Vashishta, P. Effects of Chemical Defects on Anisotropic Dielectric Response of Polyethylene. *AIP Adv.* **2019**, *9*, No. 045022.
- (34) Car, R.; Parrinello, M. Unified Approach for Molecular Dynamics and Density-Functional Theory. *Phys. Rev. Lett.* **1985**, *55*, 2471–2474.
- (35) Payne, M. C.; Teter, M. P.; Allan, D. C.; Arias, T. A.; Joannopoulos, J. D. Iterative Minimization Techniques For Ab Initio Total-Energy Calculations: Molecular Dynamics and Conjugate Gradients. *Rev. Mod. Phys.* **1992**, *64*, 1045–1097.
- (36) Kohn, W. Theory of Insulating State. *Phys. Rev.* **1964**, *133*, A171–A181.
- (37) Kohn, W.; Sham, L. J. Self-Consistent Equations Including Exchange and Correlation Effects. *Phys. Rev.* **1965**, *140*, A1133–A1138.
- (38) Perdew, J. P.; Burke, K.; Ernzerhof, M. Generalized Gradient Approximation Made Simple. *Phys. Rev. Lett.* **1996**, *77*, 3865–3868.
- (39) Grimme, S. Semiempirical GGA-Type Density Functional Constructed with a Long-Range Dispersion Correction. *J. Comput. Chem.* **2006**, *27*, 1787–1799.
- (40) Blochl, P. E. Projector Augmented-Wave Method. *Phys. Rev. B: Condens. Matter Mater. Phys.* **1994**, *50*, 17953–17979.
- (41) Shimojo, F.; Ohmura, S.; Mou, W.; Kalia, R. K.; Nakano, A.; Vashishta, P. Large Nonadiabatic Quantum Molecular Dynamics Simulations on Parallel Computers. *Comput. Phys. Commun.* **2013**, *184*, 1–8.

- (42) Shimojo, F.; et al. A Divide-Conquer-Recombine Algorithmic Paradigm for Large Spatiotemporal Quantum Molecular Dynamics Simulations. *J. Chem. Phys.* **2014**, *140*, 18A529.
- (43) Meng, S.; Kaxiras, E. Real-Time, Local Basis-Set Implementation of Time-Dependent Density Functional Theory for Excited State Dynamics Simulations. *J. Chem. Phys.* **2008**, *129*, No. 054110.
- (44) Craig, C. F.; Duncan, W. R.; Prezhdoo, O. V. Trajectory Surface Hopping in the Time-Dependent Kohn-Sham Approach for Electron-Nuclear Dynamics. *Phys. Rev. Lett.* **2005**, *95*, 163001.
- (45) Imachi, H.; Yokoyama, S.; Kaji, T.; Abe, Y.; Tada, T.; Hoshi, T. One-Hundred-Nm-Scale Electronic Structure and Transport Calculations of Organic Polymers on the K Computer. *AIP Conf. Proc.* **2016**, *1790*, No. 020010.
- (46) Runge, E.; Gross, E. K. U. Density-Functional Theory for Time-Dependent Systems. *Phys. Rev. Lett.* **1984**, *52*, 997–1000.
- (47) Tully, J. C. Molecular Dynamics with Electronic Transitions. *J. Chem. Phys.* **1990**, *93*, 1061–1071.
- (48) Granucci, G.; Persico, M. Critical Appraisal of the Fewest Switches Algorithm for Surface Hopping. *J. Chem. Phys.* **2007**, *126*, 134114.
- (49) Shimojo, F.; et al. Qxmd: An Open-Source Program for Nonadiabatic Quantum Molecular Dynamics. *SoftwareX* **2019**, *10*, 100307.